

Gluon Polarization in $e^+e^- \rightarrow t\bar{t}G$: Polar Angle Dependence and Beam Polarization Effects

S. Groote, J.G. Körner and J.A. Leyva¹

Institut für Physik, Johannes-Gutenberg-Universität,
Staudinger Weg 7, D-55099 Mainz, Germany

Abstract

We calculate the linear and circular polarization of gluons produced in conjunction with massive quarks in the annihilation process $e^+e^- \rightarrow q\bar{q}G$. The linear polarization is calculated in the hadron event plane as well as in the gluon-beam plane. Beam polarization and polar orientation effects are included in our discussion. For typical top pair production energies at the Next-Linear-Collider (NLC) the degree of linear polarization in the hadron event plane remains close to its soft gluon value of 100% over most of the energy spectrum of the gluon. The linear polarization in the gluon-beam plane is generally smaller but peaks toward the hard end of the gluon spectrum. The dependence of the linear polarization on beam polarization and on the polar orientation of the gluon is small. The circular polarization is largest for maximal gluon energies and shows a strong dependence on the longitudinal beam polarization. The longitudinal polarization of the beam may therefore be used to tune the circular polarization of the gluon. The massive quark results are compared with the corresponding results for the massless quark case.

¹on leave absence from CIF, Colombia

1 Introduction

The polarization of gluons in e^+e^- annihilation [1, 2], in deep inelastic scattering [3] and in quarkonium decays [1, 4] has been studied in a series of papers dating back to the early 1980's. Several proposals have been put forward to measure the polarization of the gluon among which is the proposal to measure azimuthal angular correlation effects in the splitting process of a polarized gluon into a pair of gluons or quarks [5]. Latter proposal has led to a beautiful confirmation of the presence of the three-gluon vertex using e^+e^- data [6] (see also [7]).

The earlier calculation of the gluon's polarization in e^+e^- annihilations had been done for massless fermions which was quite sufficient for the purposes of that period. In the meantime the situation has changed in as much as the heavy top quark has been discovered at Fermilab in 1995 whose production properties in e^+e^- annihilations will be studied in the proposed Next-Linear-Collider (NLC). In its first stage typical running energies of the NLC would extend from $t\bar{t}$ -threshold at about 350 GeV to maximal energies of about 550 GeV. It is quite clear that top mass effects cannot be neglected in this energy range even at the highest c.m. energies. It is therefore timely to redo the calculations of [1, 2] for heavy quarks and to investigate the influence of heavy quark mass effects on the polarization observables of the gluon. A first step in this direction was taken by us in [8] where we determined the linear polarization of the gluon in the process $e^+e^- \rightarrow t\bar{t}G$ taking the hadron event plane (for short: event plane) as a reference plane. In [8] we did not take into account azimuthal and polar orientation effects of the event plane relative to the beam. This is done by an appropriate polar and azimuthal averaging process. Beam polarization effects were only commented on in passing in [8].

In this paper we extend the analysis of [8] in several directions. We include beam-event orientation and beam polarization effects in our discussion. We also compute the circular polarization of the gluon induced by the parity-odd component of the hadron tensor and/or by longitudinal beam polarization effects. Finally we compute the linear polarization of the gluon in the gluon-beam plane which is obtained after an appropriate azimuthal averaging process.

Our paper is structured as follows. Sec. 2 describes the general formalism of massive quark plus gluon production in e^+e^- annihilations including beam and gluon polarization effects. Our production cross section is written in terms of three modular building blocks. The first building block defines the orientation of the lepton beam relative to the hadron plane and the dependence on the polarization parameters of the beam. The second building block specifies the electro-weak model dependence and the third building block specifies the QCD dynamics in terms of a set of polarized and unpolarized structure functions. In Sec. 3 we list our results for the twice-differential $O(\alpha_s)$ polarized and unpolarized structure functions as well as closed form expressions for their once- and twice-integrated forms. Sec. 4 contains

our numerical results. We provide plots of the energy dependence of the linear and circular polarization of the gluon, their polar angle dependence and their beam polarization dependence. In Sec. 5 we discuss the linear polarization of the gluon in the gluon-beam plane which can be obtained via an azimuthal rotation from the event plane. Sec. 6 contains our summary and our conclusions.

Before we get to the main topic of this paper we want to briefly present some numerical evidence for what is referred to as the “dead-cone” effect which occurs when soft gluons are radiated off heavy quarks. In the heavy quark case there is a depletion of gluons close to the direction of the heavy quark and the antiquark. This is quite different from the case of gluons radiated off light quarks where the production peaks towards the collinear limit. Large angle emission is a welcome effect in e^+e^- annihilation since gluons emitted at large angles from the heavy quark and antiquark directions are easier to reconstruct. If one is far enough away from the production threshold with sufficient velocities of the heavy quark and antiquark the decay products of the heavy quark and antiquark would tend to go along the original production direction and would thus stay away from the large-angle soft gluons radiated from the heavy quark and antiquark. For example, at $\sqrt{q^2} = 500 \text{ GeV}$ and $\sqrt{q^2} = 1000 \text{ GeV}$ one has a quark (or antiquark) velocity of $v = 0.71$ and $v = 0.94$, respectively.

In order to display the “dead-cone” effect we have plotted the quark/gluon opening angle distribution at a c.m. energy of $\sqrt{q^2} = 500 \text{ GeV}$ for four different soft gluon energies in Fig. 1(a). The quark gluon opening angle θ_{13} is given by

$$\cos \theta_{13} = \frac{x^2 + (2-x)w}{x\sqrt{(2-x+w)^2 - 4\xi}} \quad (1)$$

At these low energies there is in fact a depletion of gluons radiated at small opening angles. However, the distributions rise uniformly to their maximum values at 90° and do not show a peak at around $\theta_{13} = 2m/\sqrt{q^2} = 40.10^\circ$ as predicted in [10]. In Fig. 1(b) we show the opening angle distribution for gluons at a fixed energy of $E = 6 \text{ GeV}$ for three different values of the c.m. energy. Again there is a depletion of gluons radiated at small opening angles for all three c.m. energies. The $\sqrt{q^2} = 1000 \text{ GeV}$ opening angle distribution does show a peak at around $\theta_{13} = 40^\circ$ which is somewhat displaced from the peak position $\theta_{13} = 20.05^\circ$ as calculated from the above relation. The two distributions at lower c.m. energies do not show any peak structure but rise uniformly to their maximum values at 90° .

We mention that some indirect evidence for the “dead-cone” effect was presented in [11] where we calculated the mean transverse momentum of the top with regard to the antitop direction in e^+e^- annihilations. The mean transverse momentum of the top was found to be only slightly below the mean gluon energy in the whole range from $t\bar{t}$ -threshold to 1000 GeV . Since the transverse momentum of the top

has to be balanced by the transverse momentum of the gluon the near equality of the two means implies large mean opening angles for the gluon.

2 General formalism

As is usual we shall represent the two-by-two differential density matrix $d\sigma = d\sigma_{\lambda_G \lambda'_G}$ of the gluon with gluon helicities $\lambda_G = \pm 1$ in terms of its components along the unit matrix and the three Pauli matrices. Accordingly one has

$$d\sigma = \frac{1}{2}(d\sigma \mathbb{1} + d\sigma^x \sigma_x + d\sigma^y \sigma_y + d\sigma^z \sigma_z), \quad (2)$$

where $d\sigma$ is the unpolarized differential rate and $d\vec{\sigma} = (d\sigma^x, d\sigma^y, d\sigma^z)$ are the three components of the (unnormalized) differential Stokes vector. In this paper the (x, y, z) -components of the Stokes vector will mostly be referred to the event plane such that the gluon points in the z -direction and the $(q\bar{q}G)$ -plane defines the (x, z) -plane (for short: event plane). An exception is Sec. 5 where the linear polarization of the gluon is calculated in the gluon-beam plane.

Specifying to $e^+e^- \rightarrow q(p_1)\bar{q}(p_2)G(p_3)$ we perform an azimuthal averaging over the relative beam-event orientation. After azimuthal averaging the y -component of the Stokes vector $d\sigma^y$ drops out [1, 2]². One retains only the x - and z -components of the Stokes vector which are referred to as the gluon's linear polarization in the event plane and the circular polarization of the gluon, respectively. The differential unpolarized and polarized rates, differential with regard to the polar beam-event orientation and the two energy-type variables $x = 2p_3 \cdot q/q^2$ and $w = 2(p_1 - p_2) \cdot q/q^2$ (with $q = p_1 + p_2 + p_3$) are then given by

$$\begin{aligned} \frac{d\sigma^{(x)}}{d \cos \theta dx dw} &= \frac{3}{8}(1 + \cos^2 \theta) \left(g_{11} \frac{d\sigma_U^{1(x)}}{dx dw} + g_{12} \frac{d\sigma_U^{2(x)}}{dx dw} \right) \\ &+ \frac{3}{4} \sin^2 \theta \left(g_{11} \frac{d\sigma_L^{1(x)}}{dx dw} + g_{12} \frac{d\sigma_L^{2(x)}}{dx dw} \right) + \frac{3}{4} \cos \theta g_{44} \frac{d\sigma_F^{4(x)}}{dx dw}, \end{aligned} \quad (3)$$

$$\frac{d\sigma^z}{d \cos \theta dx dw} = \frac{3}{8}(1 + \cos^2 \theta) g_{14} \frac{d\sigma_U^{4z}}{dx dw} + \frac{3}{4} \cos \theta \left(g_{41} \frac{d\sigma_F^{1z}}{dx dw} + g_{42} \frac{d\sigma_F^{2z}}{dx dw} \right). \quad (4)$$

The notation $d\sigma^{(x)}$ stands for either $d\sigma$ or $d\sigma^x$, and the same for $d\sigma_\alpha^{i(x)}$ (the indices $i = 1, 2, 4$ and $\alpha = U, L, F$ are explained later on). The notation closely follows the one used in [6]. Noteworthy is the absence of a longitudinal contribution to the

²The linear gluon-beam plane polarization observable of the gluon discussed in Sec. 5 involves a different azimuthal averaging process. For this application one needs to retain one particular y -component of the Stokes vector in the event plane.

circular polarization with an angular $\sin^2 \theta$ -dependence. This is a tree-level effect due to the CP -evenness of the Standard Model interactions.

We have written the electro-weak cross section in modular form in terms of three building blocks. The first building block determines the angular beam-event dependence. For the case at hand one remains with a polar angle dependence after azimuthal integration, where θ is the polar angle between the gluon and the electron beam. The second building block specifies the electro-weak model dependence through the parameters g_{ij} ($i, j = 1, \dots, 4$). They are given by

$$\begin{aligned}
g_{11} &= Q_f^2 - 2Q_f v_e v_f \operatorname{Re} \chi_Z + (v_e^2 + a_e^2)(v_f^2 + a_f^2) |\chi_Z|^2, \\
g_{12} &= Q_f^2 - 2Q_f v_e v_f \operatorname{Re} \chi_Z + (v_e^2 + a_e^2)(v_f^2 - a_f^2) |\chi_Z|^2, \\
g_{14} &= 2Q_f v_e a_f \operatorname{Re} \chi_Z - 2(v_e^2 + a_e^2) v_f a_f |\chi_Z|^2, \\
g_{41} &= 2Q_f a_e v_f \operatorname{Re} \chi_Z - 2v_e a_e (v_f^2 + a_f^2) |\chi_Z|^2, \\
g_{42} &= 2Q_f a_e v_f \operatorname{Re} \chi_Z - 2v_e a_e (v_f^2 - a_f^2) |\chi_Z|^2, \\
g_{44} &= -2Q_f a_e a_f \operatorname{Re} \chi_Z + 4v_e a_e v_f a_f |\chi_Z|^2,
\end{aligned} \tag{5}$$

where, in the Standard Model, $\chi_Z(q^2) = gM_Z^2 q^2 / (q^2 - M_Z^2 + iM_Z \Gamma_Z)$, with M_Z and Γ_Z the mass and width of the Z^0 and $g = G_F(8\sqrt{2}\pi\alpha)^{-1} \approx 4.49 \cdot 10^{-5} \text{ GeV}^{-2}$. Q_f are the charges of the final state quarks; v_e and a_e , v_f and a_f are the electro-weak vector and axial vector coupling constants. For example, in the Weinberg-Salam model, one has $v_e = -1 + 4 \sin^2 \theta_W$, $a_e = -1$ for leptons, $v_f = 1 - \frac{8}{3} \sin^2 \theta_W$, $a_f = 1$ for up-type quarks ($Q_f = \frac{2}{3}$), and $v_f = -1 + \frac{4}{3} \sin^2 \theta_W$, $a_f = -1$ for down-type quarks ($Q_f = -\frac{1}{3}$). In this paper we use Standard Model couplings with $\sin^2 \theta_W = 0.226$.

The third building block, finally, is given by the hadron dynamics, i.e. by the current-induced production of a heavy quark pair with subsequent gluon emission. The QCD dynamics is encoded in the hadronic rate functions $d\sigma_\alpha^{i(x)}/dx dw$ and $d\sigma_\alpha^{iz}/dx dw$ with specific components denoted by the indices α and i , and the polarization indices x and z . The hadronic rate functions can in turn be related to the polarized and unpolarized hadronic structure functions $H_\alpha^{i(x)}$ and H_α^{iz} according to

$$\frac{d\sigma_\alpha^{i(x)}}{dx dw} = \frac{\alpha^2}{6\pi q^2} H_\alpha^{i(x)}(x, w), \quad \frac{d\sigma_\alpha^{iz}}{dx dw} = \frac{\alpha^2}{6\pi q^2} H_\alpha^{iz}(x, w). \tag{6}$$

The different hadronic structure functions are specific components of the hadronic three-body tensor $H_{\mu\nu}$ induced by the product of vector current (V) and axial vector current (A) interactions. In the case of massive quark pair production one has four different independent current products which are denoted by the upper index $i = 1, \dots, 4$, where

$$\begin{aligned}
H^1 &= \frac{1}{2}(H^{VV} + H^{AA}), & H^2 &= \frac{1}{2}(H^{VV} - H^{AA}), \\
H^3 &= \frac{i}{2}(H^{VA} - H^{AV}), & H^4 &= \frac{1}{2}(H^{VA} + H^{AV}).
\end{aligned} \tag{7}$$

We have temporarily dropped all further indices on the hadron tensor in Eq. (7).

We mention that, because of CP -invariance and because we are calculating at tree level, the linear combination H^3 does not contribute to the cross section and the spin observables considered in this paper. The lower index $\alpha = U, L, F$ specifies the relevant density matrix element of the gauge boson that determines the polar angle $\cos\theta$ -distribution. The three elements of the density matrix are referred to as the ‘‘unpolarized transverse’’ component $H_U = H_{++} + H_{--} = H_{11} + H_{22}$, the ‘‘longitudinal’’ component $H_L = H_{00}$ and the ‘‘forward-backward asymmetric’’ component $H_F = H_{++} - H_{--} = -i(H_{12} - H_{21})$ where we have listed both the spherical and Cartesian components of the relevant density matrix elements. The three (U, L, F) components can be obtained from the full hadron tensor $H_{\mu\nu}$ by covariant contraction as discussed in [6]. The unpolarized hadronic tensor H_α^i and the polarized hadronic tensors H_α^{ix} and H_α^{iz} are defined in exact analogy to Eq. (2).

Eqs. (3) and (4) give the differential cross section for unpolarized beams. The case of longitudinally polarized beams can easily be included. For the unpolarized and linearly polarized rates $d\sigma_\alpha^{i(x)}$ one has to effect the replacement

$$\begin{aligned} g_{1i} &\rightarrow (1 - h^- h^+)g_{1i} + (h^- - h^+)g_{4i} & (i = 1, 2) \\ g_{44} &\rightarrow (h^- - h^+)g_{14} + (1 - h^- h^+)g_{44} \end{aligned} \quad (8)$$

where h^+ and h^- are the degrees of the longitudinal (or helicity) polarization of the positron and electron beam, respectively. For the circularly polarized rates $d\sigma_\alpha^{iz}$ one has the replacements

$$\begin{aligned} g_{14} &\rightarrow (1 - h^- h^+)g_{14} + (h^- - h^+)g_{44} \\ g_{4i} &\rightarrow (h^- - h^+)g_{1i} + (1 - h^- h^+)g_{4i} & (i = 1, 2). \end{aligned} \quad (9)$$

Transverse beam polarization effects can also be easily included in the framework of our formalism (see e.g. [9]) but will not be further discussed in this paper.

After having described the general formalism we now go on to present explicit expressions for the polarized and unpolarized hadronic structure functions for the annihilation process $e^+e^- \rightarrow q\bar{q}G$ in the following section.

3 Polarized and unpolarized structure functions

The various components of the hadronic tensor can be easily calculated from the relevant tree level Feynman diagrams and are given by

$$\begin{aligned} H_U^1(x, w) &= -16\left(\frac{2}{x} - 2 + x\right)\frac{1}{x} - 64t_+(x, w) + 32\left(\frac{2}{x} - 2 + x\right)t_+^\ell(x, w), \\ H_U^2(x, w) &= -32\xi t_+(x, w) + 16\xi\left(\frac{2-\xi}{x} - 2\right)t_+^\ell(x, w), \end{aligned}$$

$$\begin{aligned}
H_L^1(x, w) &= 32\left(\frac{1}{x} - 1\right)\frac{1}{x} + 16\xi t_+(x, w) - 8\xi\left(\frac{6-\xi}{x} - 2 - x\right)t_+^\ell(x, w), \quad (10) \\
H_L^2(x, w) &= -16\xi t_+(x, w) + 8\xi\left(\frac{2-\xi}{x} - 2 - x\right)t_+^\ell(x, w), \\
H_F^4(x, w) &= 64t_-(x, w) - 32\left(\frac{2}{x} - 2 + x\right)t_-^\ell(x, w),
\end{aligned}$$

$$\begin{aligned}
H_U^{1x}(x, w) &= -32\left(\frac{1}{x} - 1\right)\frac{1}{x} - 64t_+(x, w) + 64\left(\frac{1}{x} - 1\right)t_+^\ell(x, w), \\
H_U^{2x}(x, w) &= -32\xi t_+(x, w) + 16\xi\left(\frac{2-\xi}{x} - 2\right)t_+^\ell(x, w), \\
H_L^{1x}(x, w) &= 32\left(\frac{1}{x} - 1\right)\frac{1}{x} + 16\xi t_+(x, w) - 8\xi\left(\frac{6-\xi}{x} - 2\right)t_+^\ell(x, w), \quad (11) \\
H_L^{2x}(x, w) &= -16\xi t_+(x, w) + 8\xi\left(\frac{2-\xi}{x} - 2\right)t_+^\ell(x, w), \\
H_F^{4x}(x, w) &= 64t_-(x, w) - 64\left(\frac{1}{x} - 1\right)t_-^\ell(x, w),
\end{aligned}$$

$$\begin{aligned}
H_U^{4z}(x, w) &= 64xt_-(x, w) - 32(2-x)t_-^\ell(x, w), \\
H_L^{4z}(x, w) &= 0, \\
H_F^{1z}(x, w) &= -16(2-x)\frac{1}{x} - 64xt_+(x, w) + 32(2-x)t_+^\ell(x, w), \quad (12) \\
H_F^{2z}(x, w) &= 0
\end{aligned}$$

with $\xi = 4m_q^2/q^2$, where we have used the abbreviations

$$t_\pm(x, w) := \frac{\xi}{4} \left(\frac{1}{(x-w)^2} \pm \frac{1}{(x+w)^2} \right), \quad t_\pm^\ell(x, w) := \frac{1}{2} \left(\frac{1}{x-w} \pm \frac{1}{x+w} \right). \quad (13)$$

We mention that the vanishing of the hadron tensor components $H_L^{4z}(x, w)$ and $H_F^{2z}(x, w)$ is a tree-level effect and is due to the CP -invariance of the underlying Standard Model interaction.

Note that under quark-antiquark exchange (charge conjugation) $t_\pm \rightarrow \pm t_\pm$ and $t_\pm^\ell \rightarrow \pm t_\pm^\ell$. This implies that the charge conjugation odd contributions t_- and t_-^ℓ vanish if one does not discriminate between quarks and antiquarks. In the following we wish to distinguish between the cases where the quark flavours are identified or not identified and we will refer to these two cases as the flavour tag and flavour no-tag cases, respectively.

Let us briefly pause to discuss the mass zero limit of the hadronic tensor components. The mass zero limit can easily be taken by setting $\xi = 0$ in Eqs. (10–12). From the terms that remain after taking the $\xi \rightarrow 0$ limit it is only the terms proportional to $t_\pm^\ell(x, w)$ that are important, because they are mass singular in the $\xi \rightarrow 0$

limit. In fact, when one performs the w -integration including flavour-tagging, the mass singular functions $t_{\pm}^{\ell}(x, w)$ integrate to an x -independent logarithmic factor and a finite (x -dependent) term, i.e. $\int t_{\pm}^{\ell}(x, w)dw \rightarrow -\ln \xi + c_{\pm}$ (see Eq. (13)). Keeping only the dominant logarithmic term one has in the $\xi \rightarrow 0$ limit

$$\begin{aligned} H_U^1(x) &\rightarrow -32\left(\frac{2}{x} - 2 + x\right) \ln \xi, & H_F^4(x) &\rightarrow 32\left(\frac{2}{x} - 2 + x\right) \ln \xi, \\ H_U^{1x}(x) &\rightarrow -64\left(\frac{1}{x} - 1\right) \ln \xi, & H_F^{4x}(x) &\rightarrow 64\left(\frac{1}{x} - 1\right) \ln \xi, \\ H_U^{4z}(x) &\rightarrow 32(2 - x) \ln \xi, & H_F^{1z}(x) &\rightarrow -32(2 - x) \ln \xi. \end{aligned} \quad (14)$$

The remaining terms in Eqs. (10–12) are subdominant. The expressions in Eqs. (14) determine the energy dependence of the linear and circular polarization of the gluon in the mass zero limit. They will be used later on to compare with the corresponding expressions in the massive case.

Returning to the case of massive quarks, the integration over the phase-space parameter w can be easily done. However, as mentioned earlier on, C -odd observables average out to zero in this integration if one does not employ flavour-tagging. For example, the contributions to the circular polarization vanish when we integrate over the whole range of w since the integration variable is antisymmetric in the quark and antiquark variables. Nonvanishing values of the circular polarization are obtained only if one applies flavour-tagging, i.e. one has to take care to distinguish between quark and antiquark energies in the integration. Thus, for a fixed value of the gluon's energy, one first integrates over positive values of the w -variable and then subtracts the integral over negative w -values. Or, equivalently, one just takes twice the value of the circular polarization calculated for positive w .

Let us list the few basic w -integrals that are needed in the calculation. The integration has to be done between the symmetric phase space boundaries $-w_+$ and w_+ where

$$w_+(x) = x\sqrt{\frac{1-x-\xi}{1-x}}. \quad (15)$$

One has

$$\begin{aligned} \int_{-w_+(x)}^{+w_+(x)} t_+(x, w)dw &= \left(\frac{1}{x} - 1\right)\frac{1}{x}w_+(x), \\ \int_{-w_+(x)}^{+w_+(x)} t_+^{\ell}(x, w)dw &= \ln\left(\frac{\sqrt{1-x} + \sqrt{1-x-\xi}}{\sqrt{1-x} - \sqrt{1-x-\xi}}\right) =: t_+^{\ell}(x), \\ 2 \int_0^{+w_+(x)} t_-(x, w)dw &= \frac{1-\xi}{x} - 1, \\ 2 \int_0^{+w_+(x)} t_-^{\ell}(x, w)dw &= \ln\left(\frac{1-x}{\xi}\right) =: t_-^{\ell}(x). \end{aligned} \quad (16)$$

where we have employed flavour-tagging for the last two C -odd integrals as discussed before. Using these basic integrals we obtain the once-integrated structure functions $H_\alpha^i(x)$, $H_\alpha^{ix}(x)$ and $H_\alpha^{iz}(x)$. One has

$$\begin{aligned}
H_U^1(x) &= -32\left(\frac{4}{x} - 4 + x\right)\frac{1}{x}w_+(x) + 32\left(\frac{2}{x} - 2 + x\right)t_+^\ell(x), \\
H_U^2(x) &= -32\xi\left(\frac{1}{x} - 1\right)\frac{1}{x}w_+(x) + 16\xi\left(\frac{2-\xi}{x} - 2\right)t_+^\ell(x), \\
H_L^1(x) &= 16(4 + \xi)\left(\frac{1}{x} - 1\right)\frac{1}{x}w_+(x) - 8\xi\left(\frac{6-\xi}{x} - 2 - x\right)t_+^\ell(x), \\
H_L^2(x) &= -16\xi\left(\frac{1}{x} - 1\right)\frac{1}{x}w_+(x) + 8\xi\left(\frac{2-\xi}{x} - 2 - x\right)t_+^\ell(x), \\
H_F^4(x) &= 64\left(\frac{1-\xi}{x} - 1\right) - 32\left(\frac{2}{x} - 2 + x\right)t_-^\ell(x),
\end{aligned} \tag{17}$$

$$\begin{aligned}
H_U^{1x}(x) &= -128\left(\frac{1}{x} - 1\right)\frac{1}{x}w_+(x) + 64\left(\frac{1}{x} - 1\right)t_+^\ell(x) \\
H_U^{2x}(x) &= -32\xi\left(\frac{1}{x} - 1\right)\frac{1}{x}w_+(x) + 16\xi\left(\frac{2-\xi}{x} - 2\right)t_+^\ell(x), \\
H_L^{1x}(x) &= 16(4 + \xi)\left(\frac{1}{x} - 1\right)\frac{1}{x}w_+(x) - 8\xi\left(\frac{6-\xi}{x} - 2\right)t_+^\ell(x), \\
H_L^{2x}(x) &= -16\xi\left(\frac{1}{x} - 1\right)\frac{1}{x}w_+(x) + 8\xi\left(\frac{2-\xi}{x} - 2\right)t_+^\ell(x), \\
H_F^{4x}(x) &= 64\left(\frac{1-\xi}{x} - 1\right) - 64\left(\frac{1}{x} - 1\right)t_-^\ell(x),
\end{aligned} \tag{18}$$

$$H_U^{4z}(x) = 64(1 - \xi - x) - 32(2 - x)t_-^\ell(x),$$

$$H_L^{4z}(x) = 0,$$

$$H_F^{1z}(x) = -32(4 - 3x)\frac{1}{x}w_+(x) + 32(2 - x)t_+^\ell(x), \tag{19}$$

$$H_F^{2z}(x) = 0.$$

Our notation is such that $H(x) = \int H(x, w)dw$. The dominant leading logarithmic $\ln \xi$ terms in the zero mass limit derive from the logarithmic functions $t_+^\ell(x)$ and $t_-^\ell(x)$ and have been listed before in Eq. (14).

The last step is the integration over the second phase-space parameter x . It is clear that we have to introduce a gluon energy cutoff at the soft end of the gluon spectrum in order to keep the rate finite. Denoting the cutoff energy by $E_c = \lambda\sqrt{q^2}$ the integration extends from $x = 2\lambda = 2E_c/\lambda\sqrt{q^2}$ to $x = 1 - \xi$. We obtain

$$H_U^1 = -128\mathcal{G}(-1) + 128\mathcal{G}(0) - 32\mathcal{G}(1) + 64\mathcal{G}_\ell(-1) - 64\mathcal{G}_\ell(0) + 32\mathcal{G}_\ell(1),$$

$$\begin{aligned}
H_U^2 &= -32\xi\mathcal{G}(-1) + 32\xi\mathcal{G}(0) + 16\xi(2 - \xi)\mathcal{G}_\ell(-1) - 32\xi\mathcal{G}_\ell(0), \\
H_L^1 &= 16(4 + \xi)\mathcal{G}(-1) - 16(4 + \xi)\mathcal{G}(0) - 8\xi(6 - \xi)\mathcal{G}_\ell(-1) + 16\xi\mathcal{G}_\ell(0) + 8\xi\mathcal{G}_\ell(1), \\
H_L^2 &= -16\xi\mathcal{G}(-1) + 16\xi\mathcal{G}(0) + 8\xi(2 - \xi)\mathcal{G}_\ell(-1) - 16\xi\mathcal{G}_\ell(0) - 8\xi\mathcal{G}_\ell(1), \quad (20) \\
H_F^4 &= -8(13 - 12\xi - \xi^2 - 8\text{Li}_2(1 - \xi)) - 48 \ln \xi - 64(1 - \xi + \ln \xi) \ln \left(\frac{2\lambda}{v^2} \right),
\end{aligned}$$

$$\begin{aligned}
H_U^{1x} &= -128\mathcal{G}(-1) + 128\mathcal{G}(0) + 64\mathcal{G}_\ell(-1) - 64\mathcal{G}_\ell(0), \\
H_U^{2x} &= -32\xi\mathcal{G}(-1) + 32\xi\mathcal{G}(0) + 16\xi(2 - \xi)\mathcal{G}_\ell(-1) - 32\xi\mathcal{G}_\ell(0), \\
H_L^{1x} &= 16(4 + \xi)\mathcal{G}(-1) - 16(4 + \xi)\mathcal{G}(0) - 8\xi(6 - \xi)\mathcal{G}_\ell(-1) + 16\xi\mathcal{G}_\ell(0), \quad (21) \\
H_L^{2x} &= -16\xi\mathcal{G}(-1) + 16\xi\mathcal{G}(0) + 8\xi(2 - \xi)\mathcal{G}_\ell(-1) - 16\xi\mathcal{G}_\ell(0), \\
H_F^{4x} &= -64(2(1 - \xi) - \text{Li}_2(1 - \xi)) - 64 \ln \xi - 64(1 - \xi + \ln \xi) \ln \left(\frac{2\lambda}{v^2} \right),
\end{aligned}$$

$$\begin{aligned}
H_U^{4z} &= 24(1 - \xi)(3 - \xi) + 48 \ln \xi, \\
H_L^{4z} &= 0, \quad (22) \\
H_F^{1z} &= -128\mathcal{G}(0) + 96\mathcal{G}(1) + 64\mathcal{G}_\ell(0) - 32\mathcal{G}_\ell(1), \\
H_F^{2z} &= 0
\end{aligned}$$

where

$$\mathcal{G}(m) := \int_{2\lambda}^{1-\xi} x^{m-1} w_+(x) dx. \quad (23)$$

Full analytical results for the integrals have been given before in [8]. Here we employ a small λ -expansion and retain only the leading $\ln \lambda$ and the next-to-leading constant contributions in the small λ -expansion. One has

$$\mathcal{G}(-1) = -\ln \left(\frac{1+v}{1-v} \right) - v \ln \left(\frac{\lambda\xi}{2v^2} \right), \quad (24)$$

$$\mathcal{G}(0) = v - \frac{1}{2}\xi \ln \left(\frac{1+v}{1-v} \right), \quad (25)$$

$$\mathcal{G}(1) = \frac{1}{4}(2 + \xi)v - \frac{\xi}{8}(4 - \xi) \ln \left(\frac{1+v}{1-v} \right), \quad (26)$$

$$\mathcal{G}_\ell(m) := \int_{2\lambda}^{1-\xi} x^m t_+^\ell(x) dx, \quad (27)$$

$$\mathcal{G}_\ell(-1) = -\ln\left(\frac{1+v}{1-v}\right) \ln\left(\frac{\lambda(1+v)^2}{2v^2}\right) - \text{Li}_2\left(\frac{4v}{(1+v)^2}\right), \quad (28)$$

$$\mathcal{G}_\ell(0) = -v + \frac{1}{2}(2-\xi) \ln\left(\frac{1+v}{1-v}\right), \quad (29)$$

$$\mathcal{G}_\ell(1) = -\frac{3}{8}(2-\xi)v + \frac{1}{16}(8-8\xi+3\xi^2) \ln\left(\frac{1+v}{1-v}\right). \quad (30)$$

We have checked that the above leading and next-to-leading log expansion has sufficient accuracy for the numerical applications to be discussed in Sec. 4.

4 Numerical results

We are now in the position to discuss the various differential distributions of the polarization variables with regard to the gluon energy. The QCD dynamics is completely specified by the various hadron tensor components assembled in Eqs. (10)–(12). In order to exhibit the quark mass and flavour dependence of the gluon’s polarization we shall present results for the top, bottom and charm pair production cases in some of the figures. We begin our discussion with the linear polarization of the gluon in the hadron event plane defined by the plane spanned by the quark, antiquark and the gluon. As discussed before the linear polarization of the gluon in the event plane is determined by the normalized x -component of the Stokes vector. To start with we integrate out the polar angle dependence in the numerator and denominator of the ratio of polarized and unpolarized cross sections given in Eq. (3). One has

$$P^x(x) = \frac{d\sigma^x/dx}{d\sigma/dx}, \quad (31)$$

where $d\sigma^x/dx$ and $d\sigma/dx$ are the twice-integrated polarized and unpolarized differential cross-sections appearing in Eq. (3). In Fig. 2(a) we show the energy dependence of the linear polarization of the gluon produced in association with charm and top quark pairs at a c.m. energy of $\sqrt{q^2} = 500 \text{ GeV}$. We have chosen to rescale the scaled gluon energy x in this plot to its maximal value given by $x_{\text{max}} = 1 - \xi$. Fig. 2(a) shows that the linear polarization remains close to its maximal value of 100% at the soft gluon point over a large portion of gluon phase-space. For the top quark case the polarization remains above the value in the charm quark case when plotted against x/x_{max} ³. In Fig. 2(b) we show the differential cross section which enters in the normalization of the polarization. The differential cross section for gluons produced in conjunction with top quark pairs can be seen to be approximately one order lower than for gluons produced in conjunction with charm quark pairs.

³When the linear polarization is compared at equal gluon energies, this relation is reversed.

In Fig. 3(a) we display the linear polarization of the gluon for three different values of the c.m. energy plotted against the scaled energy variable x/x_{\max} . As the lowest c.m. energy we choose $\sqrt{q^2} = 370 \text{ GeV}$ which is far enough above $t\bar{t}$ -threshold for a perturbative treatment to be valid. The linear polarization remains quite close to its soft-gluon value of 100% over most of the available phase-space due to the fact that there is not much energy available for the gluon so close to threshold. At the hard end of the spectrum the linear polarization has to go to zero for the simple reason that one can no longer define a hadronic plane in this collinear configuration. As the c.m. energy is increased, the linear polarization decreases for a given fixed fractional energy value x/x_{\max} . For the largest c.m. energy value $\sqrt{q^2} = 1000 \text{ GeV}$ in Fig. 3(a) the linear polarization is quite close to the zero mass limiting value also shown Fig. 3(a). As discussed before, the zero mass result is determined by the collinear configurations of the gluon, i.e. by the $\ln \xi$ contributions in Eq. (14). Using the results of Eq. (14), one obtains⁴.

$$P^x(x) = \frac{2(1-x)}{2-2x+x^2}. \quad (32)$$

Note that the zero mass linear polarization no longer depends on the electro-weak model parameters, on the flavour of the produced quark or on the polarization of the beam. The electro-weak model dependence, the flavour and beam polarization dependence is the same in the numerator and in the denominator and drops out when taking the ratio. It can be checked that the electro-weak model, the flavour and beam polarization dependence of the linear polarization is quite weak also in the massive case for the c.m. energies considered here. By comparing Fig. 2(a) with Fig. 3(a) one sees that the linear polarization in the charm quark case is already quite close to the zero mass case indicating that the approach to the asymptotic value is quite fast. This also explains the closeness of the $\sqrt{q^2} = 1000 \text{ GeV}$ curve to the zero mass curve.

In Fig. 3(b) we show the differential cross section for $e^+e^- \rightarrow t\bar{t}G$ for the same three c.m. energies as in Fig. 3(a). The differential cross section decreases as the c.m. energy is increased. As expected, the decrease is governed by the usual q^2 -factor in the differential cross section.

In Fig. 4 we show the circular polarization of the gluon for the same three c.m. energies as in Fig. 3 including again the zero mass case for up-type quarks. It is clear that we are employing flavour tagging since the circular polarization would be zero otherwise. The circular polarization is positive in all four cases and peaks toward the hard end of the gluon spectrum⁵. The circular polarization is zero at the soft end of the spectrum which is simple to understand since the linear polarization

⁴The limiting value of the polarization agrees with the corresponding result Eqs.(4)–(9) in [1] (second reference) in the limit $x_0, \delta \rightarrow 0$

⁵Note that the positive value holds for $E_q \geq E_{\bar{q}}$ and becomes negative for $E_q \leq E_{\bar{q}}$.

already saturates the total polarization bound of 100% at this point. The circular polarization remains quite small over most of the range of gluon energies except for the zero mass case. The limiting zero mass behaviour is again governed by the collinear configuration determined by the $\ln \xi$ contributions in Eq. (14). One obtains

$$P^z(x) = -\frac{g_{14}}{g_{11}} \frac{x(2-x)}{2-2x+x^2} \quad (33)$$

Note that the $\sqrt{q^2} = 1000 \text{ GeV}$ curve in Fig. 4 is still a large way away from the zero mass limit indicating that the approach to asymptotia is much slower for the circular polarization than what was observed for the linear polarization.

The x -dependent factor in the mass zero formula Eq. (33) for the circular polarization starts from zero at the soft-gluon point and reaches unity at the hard end of the spectrum. Apart from the x -dependent factor the size of the circular polarization is governed by the ratio of electroweak factors $-g_{14}/g_{11}$. Above the top quark threshold the ratio $-g_{14}/g_{11}$ is only mildly q^2 -dependent but is strongly flavour dependent. For example, for $\sqrt{q^2} = 370, 500$ and 1000 GeV one finds 0.273, 0.265 and 0.257 for the up-type quarks, and 0.678, 0.670 and 0.657 for down-type quarks, respectively. From the numerical values of the ratio $-g_{14}/g_{11}$ it is clear that one generally obtains much larger values for the circular polarization of down-type quarks than for up-type quarks. In Fig. 4(b) we provide a plot of the x -dependence of the circular polarization for $\sqrt{q^2} = 1000 \text{ GeV}$ in the zero mass case for up-type and down-type quarks. The above numerical results of the ratio g_{14}/g_{11} can be clearly identified at the hard end of the spectrum. For the sake of comparison we have also plotted the corresponding curve for bottom quarks with $m_b = 4.1 \text{ GeV}$. Mass effects tend to reduce the circular polarization showing again that the approach to the asymptotic formula Eq. (33) is quite slow.

In Fig. 5(a) we display the beam polarization dependence of the circular polarization assuming that the electrons are polarized (the beam polarization dependence of the linear polarization is quite weak). The circular polarization of the gluons can be seen to be strongly dependent on beam polarization effects. One observes a strong polarization transfer effect from the helicity polarization of the electrons to the circular polarization of the gluon which can enhance the circular polarization of the gluon up to a factor of ten. In Fig. 5(b) we exhibit the beam polarization dependence of the differential cross section. The differential cross section is enhanced by about 50% for negative electron helicities and reduced by about the same amount for positive electron helicities.

In Fig. 6(a) and Fig. 6(b) we show the $\cos \theta$ -dependence of the linear and circular polarization of the gluon where we remind the reader that θ is the polar angle of the gluon relative to the electron beam. The dependence is shown for a c.m. energy of $\sqrt{q^2} = 500 \text{ GeV}$ and for three different gluon energies. The $\cos \theta$ -dependence of the linear polarization is quite weak for all three gluon energies but becomes somewhat

larger as one moves away from the soft gluon point where the $\cos\theta$ -distribution is flat. In contrast to this, the circular polarization shows a strong asymmetry effect and turns from positive to negative values as $\cos\theta$ moves from -1 to $+1$. The asymmetry effect becomes larger as the gluon becomes harder. As Fig. 6(c) shows, the pronounced asymmetry of the circular polarization results mainly from the numerator of the relevant polarization expression. The differential cross section shown in Fig. 6(c) does not possess a very pronounced $\cos\theta$ -dependence.

In Fig. 7(a) we show a plot of the average linear polarization of the gluon as a function of the c.m. energy for three different cutoff values $E_c = \lambda\sqrt{q^2} = 3, 5$ and 10 GeV. Gluon energies of this magnitude are sufficient to make the corresponding gluon jets detectable. The average linear polarization of the gluon rises steeply from threshold and quickly attains very high values above 95%. The linear polarization becomes larger for smaller values of $E_c = \lambda\sqrt{q^2}$ and tends to 100% as the cutoff parameter tends to zero. The approach to the asymptotic value $P^x = 100\%$ is, however, rather slow. We also show the average linear polarization of the gluon limit when the quark mass goes to zero for a cutoff energy of 3 GeV. The average linear polarization is smaller than in the massive case. In Fig. 7(b) we show the cutoff dependence of the total cross section as functions of the c.m. energy. The cross sections rise steeply from threshold and then turn over to their canonical $1/q^2$ -behaviour. The cutoff dependence of the cross section is still moderate for the three chosen cutoff values.

5 Linear polarization in the gluon-beam plane

In Secs. 2, 3 and 4 the linear polarization of the gluon has been specified relative to the event plane. A measurement of the polarization would require the reconstruction of the event plane which may not always be simple. It is much easier to determine the gluon-beam plane since the beam coordinates are known a priori. In order to determine the (unnormalized) components of the Stokes vector in the gluon-beam plane one needs to rotate the event plane Stokes vector around the gluon momentum axis by the azimuthal angle χ between the two planes. One obtains⁶

$$\begin{aligned} H^{x'} &= \cos 2\chi H^x - \sin 2\chi H^y \\ H^{y'} &= \sin 2\chi H^x + \cos 2\chi H^y \\ H^{z'} &= H^z \end{aligned} \tag{34}$$

where $(H^{x'}, H^{y'}, H^{z'})$ are the components of the Stokes vector in the gluon-beam plane. Since one is rotating around the gluon axis, the circular component H^z is not

⁶Note that the Stokes vector is not a true vector and thus its transformation behaviour under rotations differs from that of a true three-vector.

affected by this rotation. We have dropped all further indices on the hadron tensor in Eq. (34).

We shall not write down the full polar $\cos\theta$ - and azimuthal χ -dependence of the polarized cross section in the new system but shall rather completely integrate out the polar and azimuthal angle dependence. One then obtains

$$\begin{aligned} H_T^{x'} &= -\frac{1}{2}(H_T^x + H_4^y) \\ H_T^{y'} &= 0 \end{aligned} \quad (35)$$

where the y' -component $H^{y'}$ drops out after azimuthal averaging. The hadron tensor components “ T ” and “ 4 ” on the right hand side are still specified in the event system and are given by (see [9])

$$\begin{aligned} H_T^x &= \frac{1}{2}(H_{+-}^x + H_{-+}^x) = \frac{1}{2}(-H_{11}^x + H_{22}^x) \\ H_4^y &= -\frac{1}{2}(H_{+-}^y - H_{-+}^y) = -\frac{1}{2}(H_{12}^y + H_{21}^y). \end{aligned} \quad (36)$$

Again these components can be calculated from the relevant tree-level Feynman diagrams. One finds

$$\begin{aligned} H_T^{1x'}(x, w) &= \frac{8}{x^2} + 8\xi t_+(x, w) - 4\xi \frac{4-\xi}{x} t_+^\ell(x, w) \\ H_T^{2x'}(x, w) &= 0. \end{aligned} \quad (37)$$

Since we are interested in the energy dependence of the linear polarization, we also give their once-integrated forms. One has

$$\begin{aligned} H_T^{1x'}(x) &= 8 \left(\frac{2+\xi}{x} - \xi \right) \frac{w_+(x)}{x} - 4\xi \frac{4-\xi}{x} t_+^\ell(x) \\ H_T^{2x'}(x) &= 0. \end{aligned} \quad (38)$$

It is quite evident that $H_T^{x'}$ has a smooth zero mass limit, i.e. there is no collinear singularity in the (x, w) -dependent structure function $H_T^{x'}(x, w)$ in Eq. (37). This must be contrasted with the corresponding structure function describing the linear polarization in the event plane which possesses a collinear singularity (see Eq. (14)). We therefore anticipate that the linear polarization in the gluon-beam plane will be generally smaller than the linear polarization in the event plane and that it tends to zero in the zero mass limit.

We are now in the position to calculate the linear polarization of the gluon in the gluon-beam plane. The general expression for the linear polarization in the gluon-beam plane reads

$$P^{x'} = \frac{g_{11}H_T^{1x'} + g_{12}H_T^{2x'}}{g_{11}(H_U^1 + H_L^1) + g_{12}(H_U^1 + H_L^2)} \quad (39)$$

where we have retained the $H_T^{2x'}$ term in the numerator even though its contribution is zero.

In Fig. 8 we show the (x/x_{max}) -dependence of the linear polarization of the gluon in the gluon-beam plane for the top quark case for three different c.m. energies. The linear polarization is generally small and peaks toward the hard end of the spectrum. Also the linear polarization tends to become larger when the c.m. energy is increased. This is counterintuitive from what was said before about the absence of a collinear singularity for the polarized structure function when $v \rightarrow 1$. The approach to the limiting behaviour of $P^{x'}$ (for $v \rightarrow 1$) is, however, so slow that one is still very far away from the limiting behaviour for the c.m. energies considered in Fig. 8. Note that the linear polarization neither vanishes at the soft end of the spectrum nor at the hard end. In fact, one obtains

$$P^{x'}(x=0) = \frac{g_{11}(-2(3-v^2)v + (1-v^2)(3+v^2)t_l)}{2((3+v^2)g_{11} + 3(1-v^2)g_{12})(2v - (1+v^2)t_l)} \quad (40)$$

at the soft gluon point, where

$$v = \sqrt{1-\xi}, \quad t_l = \ln\left(\frac{1+v}{1-v}\right). \quad (41)$$

In the zero mass limit one obtains $P^{x'}(0) \rightarrow 0$ as expected. At the hard end of the spectrum for $x = x_{max} = 1 - \xi$, the linear polarization is given by

$$P^{x'}(x_{max}) = \frac{g_{11}}{(3-v^2)g_{11} - (1-v^2)g_{12}}. \quad (42)$$

Note that the mass zero limit of Eq. (42) is finite, i.e. $P^{x'}(x_{max}) \rightarrow 1/2$ as $v \rightarrow 1$. Again one would naively expect $P^{x'} \rightarrow 0$ in this limit. However, one is picking up a phase space zero in the denominator of the polarization expression at the hard gluon point which cancels the collinear singularity. The overall effect of the cancellation is that the polarization tends to a finite value as $v \rightarrow 0$. In fact, when one plots the energy dependence of the linear polarization for very small quark masses, the linear polarization tends to zero over the whole energy range, but shoots up to the value 0.5 very close to the endpoint.

6 Summary and conclusions

We have provided a detailed discussion of the linear and circular gluon polarization of gluons produced in association with heavy and light quark pairs in e^+e^- annihilations. We have studied beam polarization and polar orientation effects on the polarization of the gluon. The linear polarization of the gluon remains close to its classical soft gluon value of 100% and is only mildly dependent on the polarization

of the beam, on the polar orientation of the gluon and on the flavour of the heavy quark pair produced in association with the gluon. Quark mass effects enhance the linear polarization of the gluon when compared at the same scaled energy scaled to the maximal energy. The circular polarization of the gluon is strongly dependent on the polarization of the beam, on the polar orientation of the gluon and on the flavour of the heavy quark pair produced in association with the gluon. The dependence on these effects can be exploited to optimally tune the circular polarization of the gluon. However, to see a nonzero circular polarization of the gluon one needs to tag the flavour of the associated quark/antiquark since the circular polarization is odd under charge conjugation and averages to zero without flavour tagging. This should not be so difficult for the heavy-flavoured quarks. To actually measure the circular polarization of gluons one needs to study the fragmentation of circularly polarized gluons into polarized particles whose polarization can be measured.

If one aims to study gluon polarization effects in the splitting process $e^+e^- \rightarrow t\bar{t}G(G \rightarrow GG, q\bar{q})$, the present on-shell calculation should be sufficient to identify and discuss the leading effects of gluon polarization without having to perform a full $O(\alpha_s^2)$ calculation of $e^+e^- \rightarrow t\bar{t}GG$ and $e^+e^- \rightarrow t\bar{t}q\bar{q}$ [5].

Acknowledgements: This work is partially supported by the BMBF, FRG, under contract No. 06MZ566, and by HUCAM, EU, under contract No. CHRX-CT94-0579. The work of J.A.L. is supported by the DAAD, FRG.

References

- [1] H.A. Olsen, P. Osland and I. Øverbø,
Phys. Lett. **89 B** (1980) 221; Nucl. Phys. **B192** (1981) 33
- [2] J.G. Körner and D.H. Schiller, DESY preprint DESY-81-043 (1981)
- [3] O.E. Olsen and H.A. Olsen, Phys. Scripta **29** (1984) 12
- [4] S.J. Brodsky, T.A. DeGrand and R. Schwitters, Phys. Lett. **79 B** (1978) 255
- [5] M. Bengtsson and P.M. Zerwas, Phys. Lett. **208 B** (1988) 306;
M. Bengtsson, Z. Phys. **C42** (1989) 75;
S. Bethke, A. Richter and P. Zerwas, Z. Phys. **C49** (1991) 59
- [6] B. Adeva *et al.*, L3 Collaboration, Phys. Lett. **248 B** (1990) 227
- [7] D. Decamp *et al.*, ALEPH Collaboration, Phys. Lett. **284 B** (1992) 163;
P. Abreu *et al.*, DELPHI Collaboration, Z. Phys. **C59** (1993) 357;

- R. Akers *et al.*, OPAL Collaboration, Z. Phys. **C65** (1995) 367;
R. Barate *et al.*, ALEPH Collaboration, CERN-PPE/97-002
- [8] S. Groote, J.G. Körner and J.A. Leyva, Phys. Rev. **D56** (1997) 6031
- [9] S. Groote, J.G. Körner and M.M. Tung, Z. Phys. **C74** (1997) 615
- [10] Yu.L. Dokshitzer, V.A. Khoze and S.I. Troyan, in Proc. 6th Int. Conf. “Physics in Collision”, ed. M. Derrick (World Scientific, Singapore, 1987), p. 417;
R. Barlow *et al.*, J. Phys. **G17** (1991) 1605
- [11] S. Groote, J.G. Körner and J.A. Leyva, “On the rigidity of back-to-back top quark pairs in e^+e^- annihilation”, Report No. MZ-TH/97-39, hep-ph/9801255, to be published in Nucl. Phys. B

Figure Captions

- Fig. 1: Quark-gluon opening angle distribution for soft gluons illustrating the “dead-cone” effect
 (a) opening angle distribution at a fixed c.m. energy of $\sqrt{q^2} = 500 \text{ GeV}$ for gluon energies of 0.5, 1, 2, and 3 GeV
 (b) opening angle distribution for a fixed gluon energy of 6 GeV at three different c.m. energies of 370, 500, and 1000 GeV
- Fig. 2: (a) energy dependence of the linear polarization of the gluon in the event plane
 (b) energy dependence of the differential cross section $e^+e^- \rightarrow t\bar{t}G$ and $e^+e^- \rightarrow c\bar{c}G$
- Fig. 3: (a) energy dependence of the linear polarization of the gluon in the event plane for different c.m. energies
 (b) energy dependence of the differential cross section for $e^+e^- \rightarrow t\bar{t}G$ for different c.m. energies
- Fig. 4: (a) energy dependence of the circular polarization of the gluon produced with a top quark pair and a zero mass up-type quark pair for different c.m. energies
 (b) energy dependence of the circular polarization of the gluon produced with zero mass up-type and down-type quarks and with a bottom quark pair at $\sqrt{q^2} = 1000 \text{ GeV}$
- Fig. 5: (a) energy dependence of the circular polarization of the gluon in $e^+e^-(h_-) \rightarrow t\bar{t}G$ with electron beam polarization
 (b) energy dependence of the differential cross section $e^+e^-(h_-) \rightarrow t\bar{t}G$ with electron beam polarization
- Fig. 6: (a) polar angle dependence of the linear polarization of the gluon in the event plane
 (b) polar angle dependence of the circular polarization of the gluon
 (c) polar angle dependence of the differential cross section
- Fig. 7: (a) Mean linear polarization of the gluon in the event plane plotted against the c.m. energy for different cutoff energies
 (b) total cross section for $e^+e^- \rightarrow t\bar{t}G$ plotted against the c.m. energy for different cutoff energies
- Fig. 8: Energy dependence of the linear polarization of the gluon in the gluon-beam plane

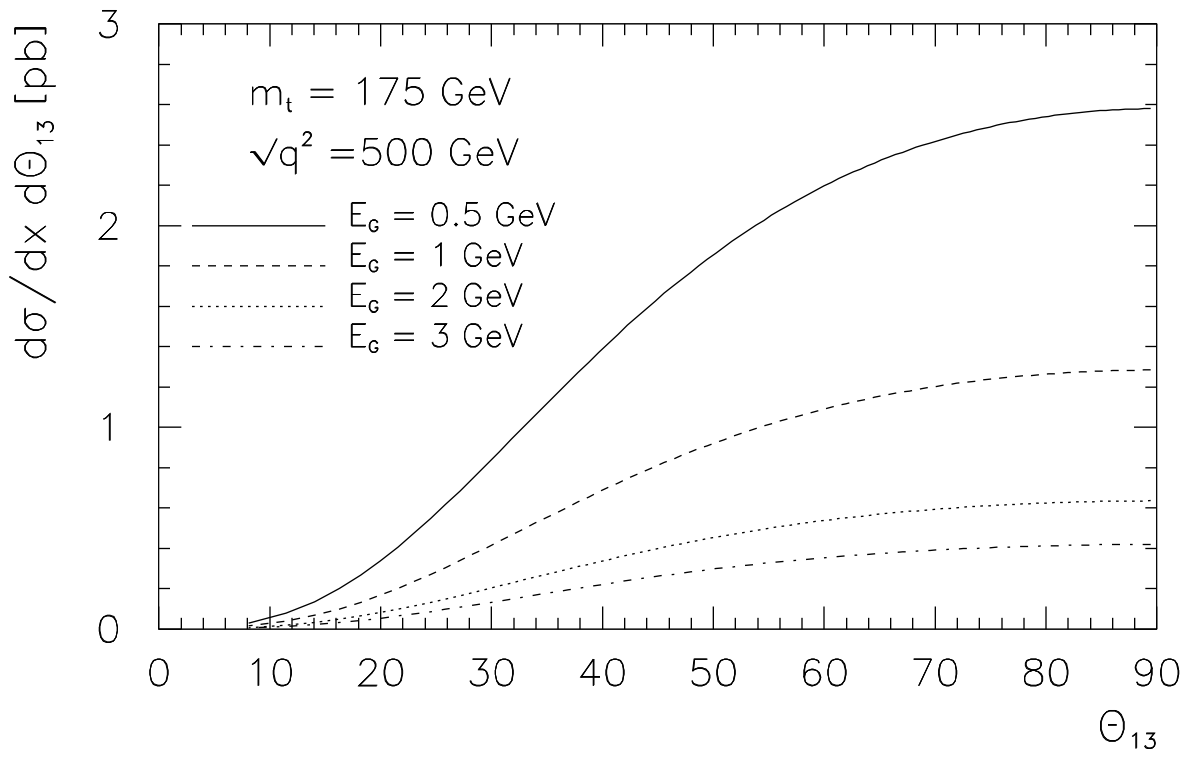


Figure 1(a)

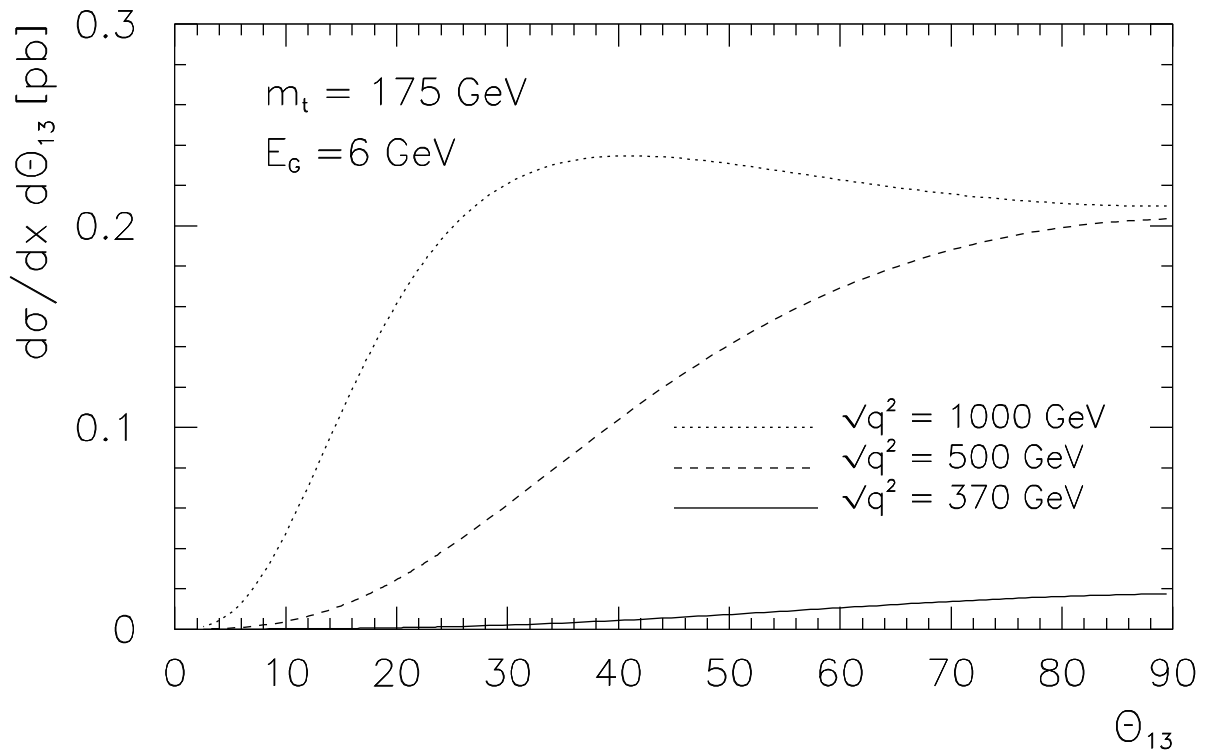


Figure 1(b)

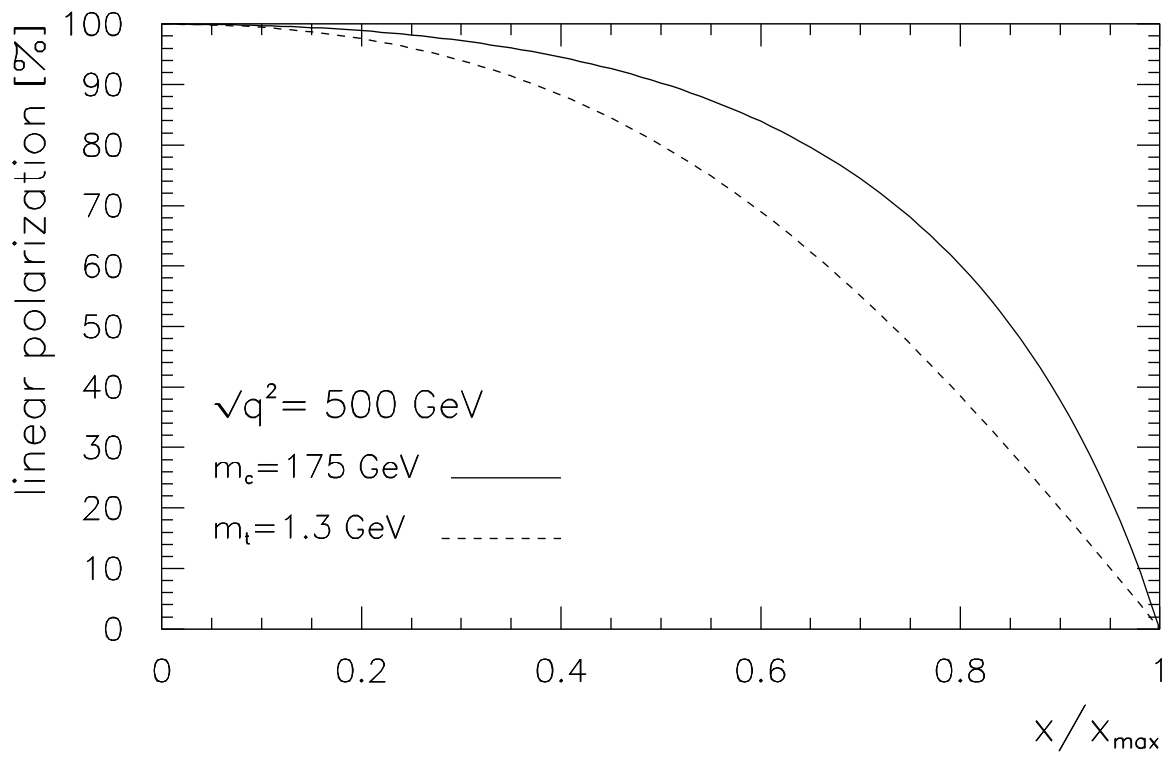


Figure 2(a)

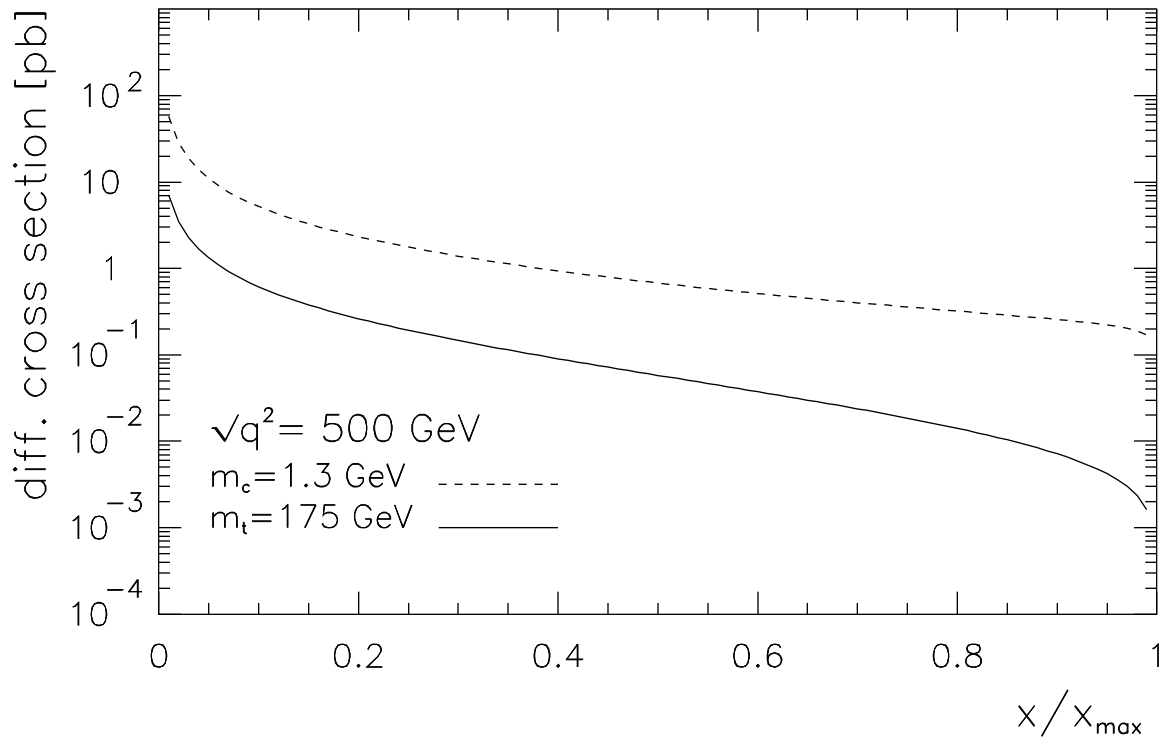


Figure 2(b)

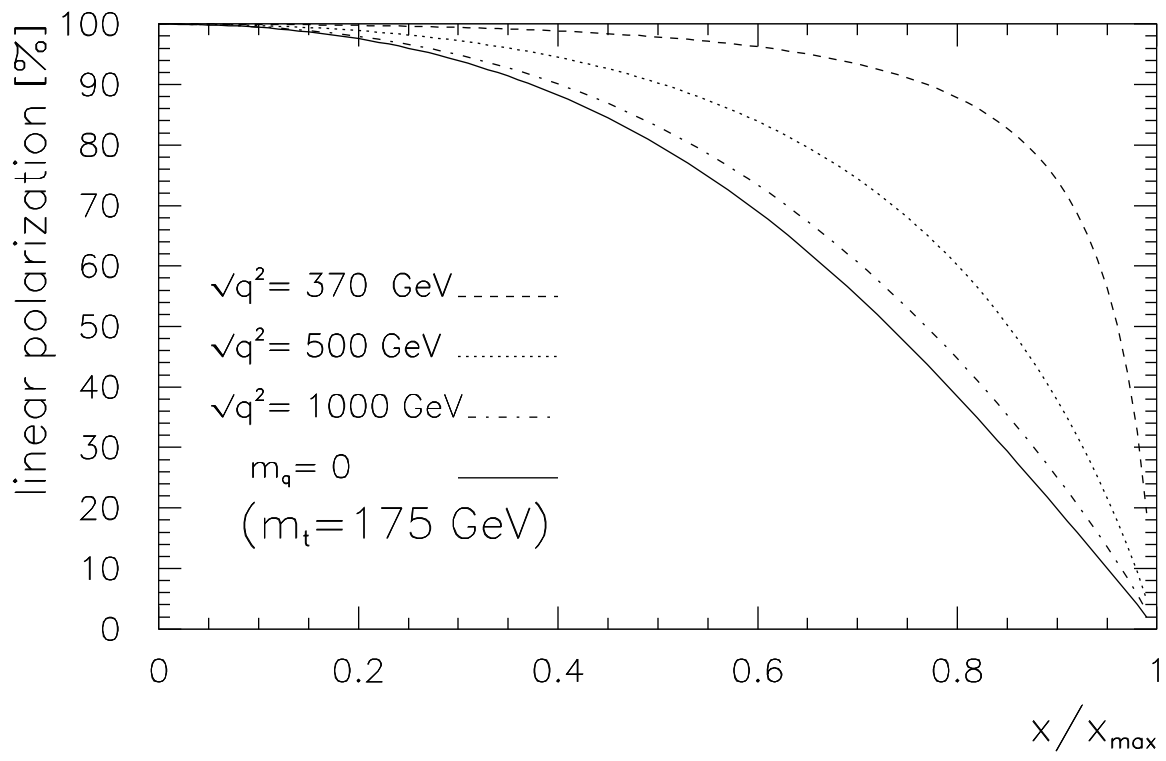


Figure 3(a)

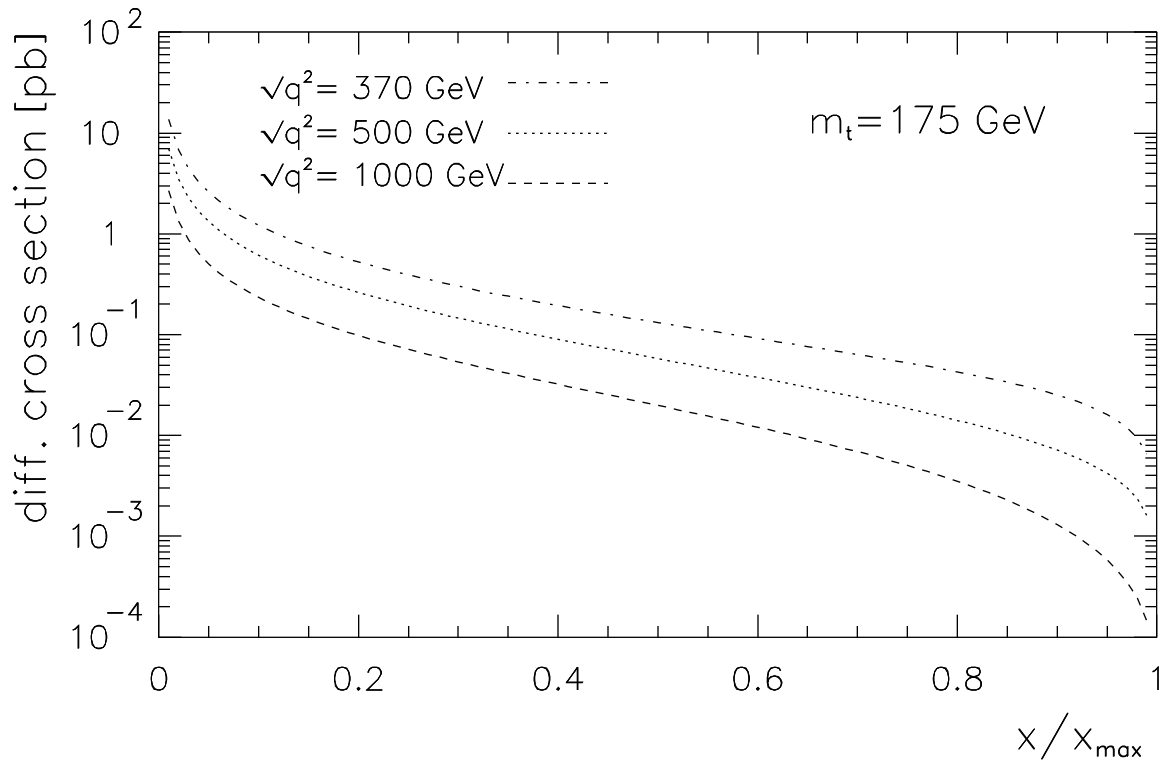


Figure 3(b)

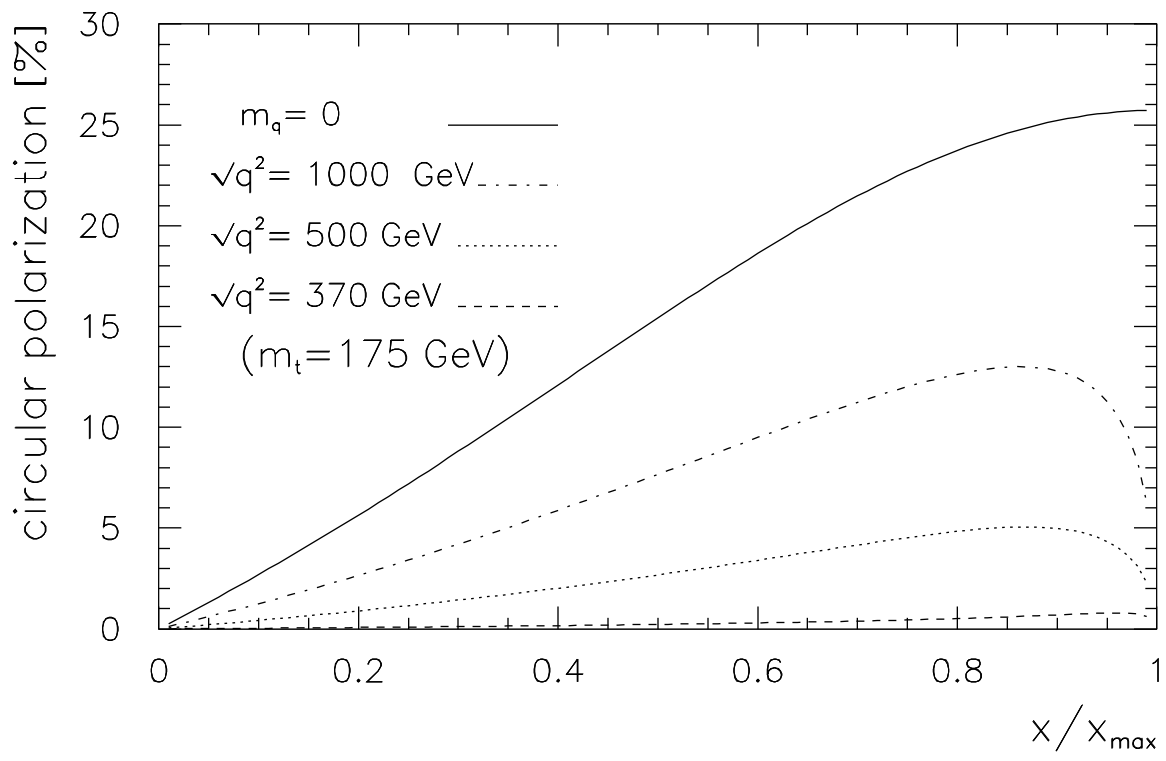


Figure 4(a)

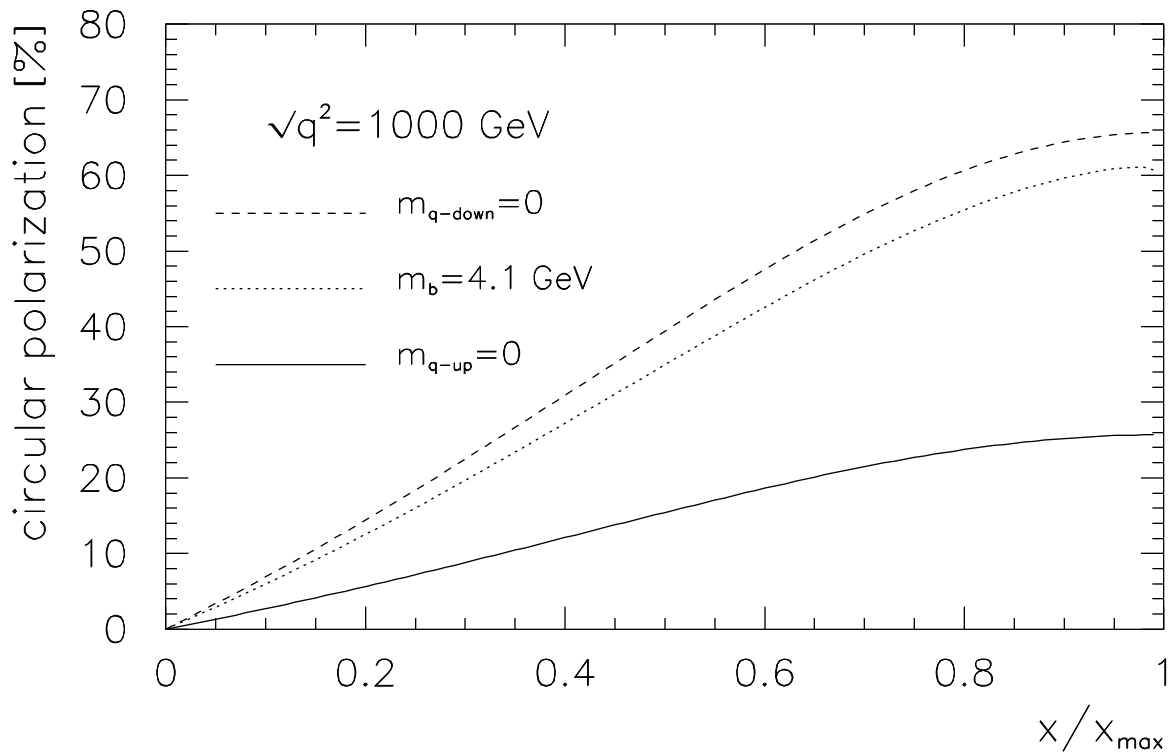


Figure 4(b)

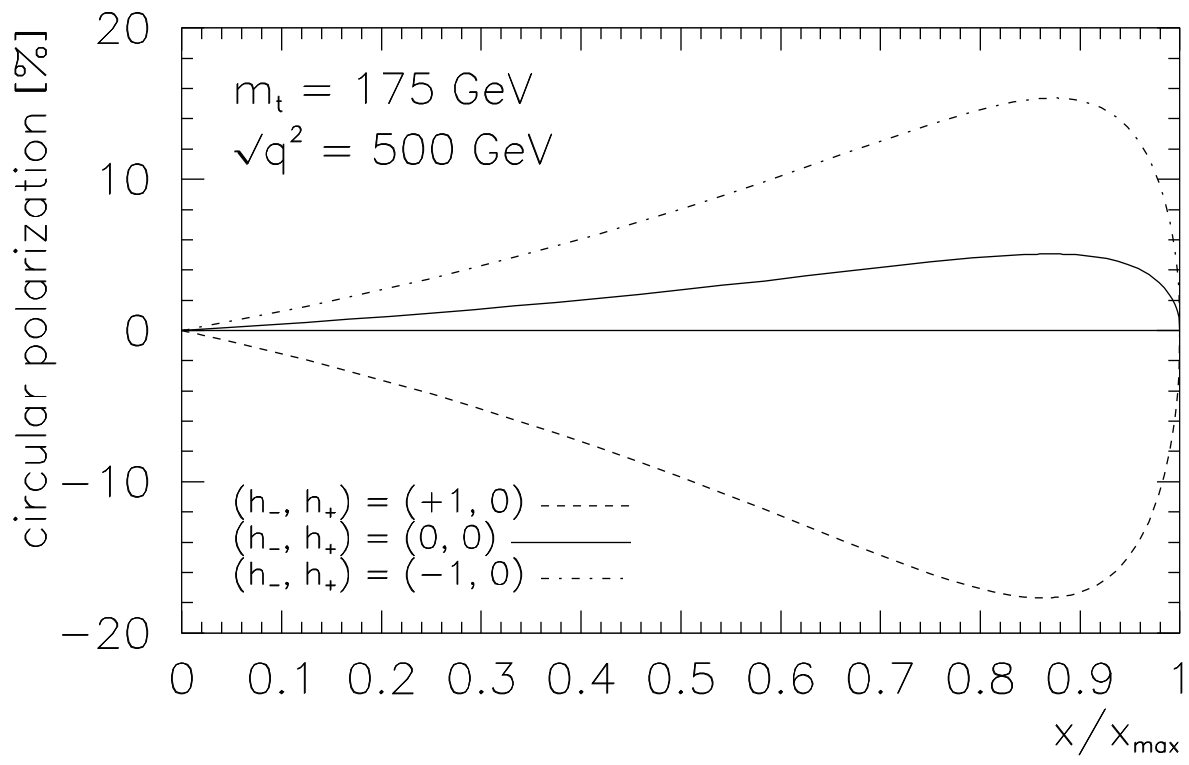


Figure 5(a)

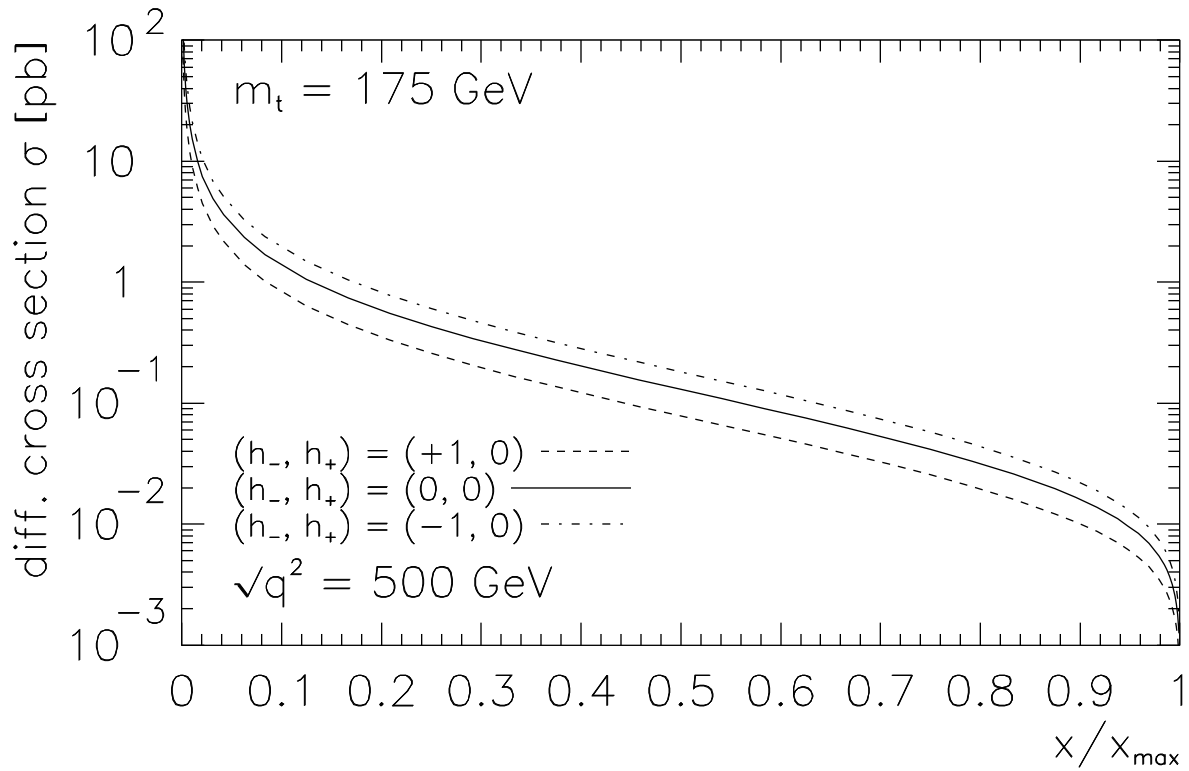


Figure 5(b)

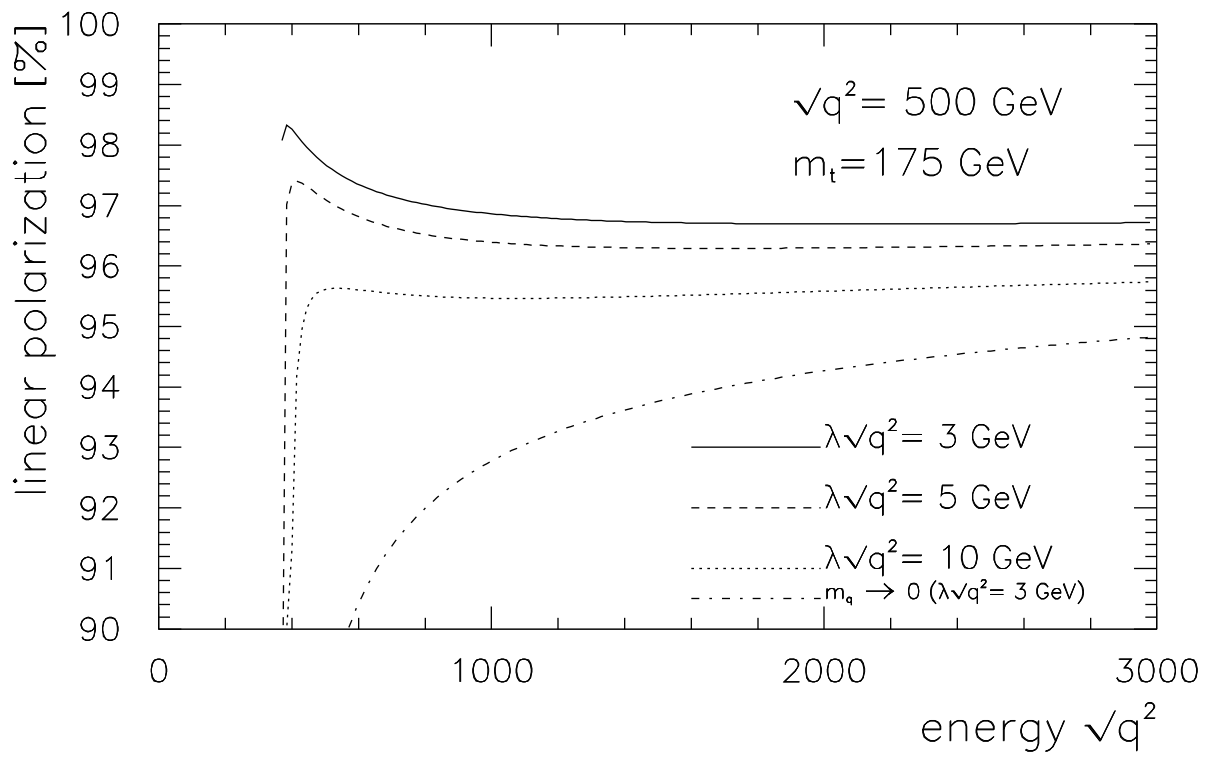


Figure 7(a)

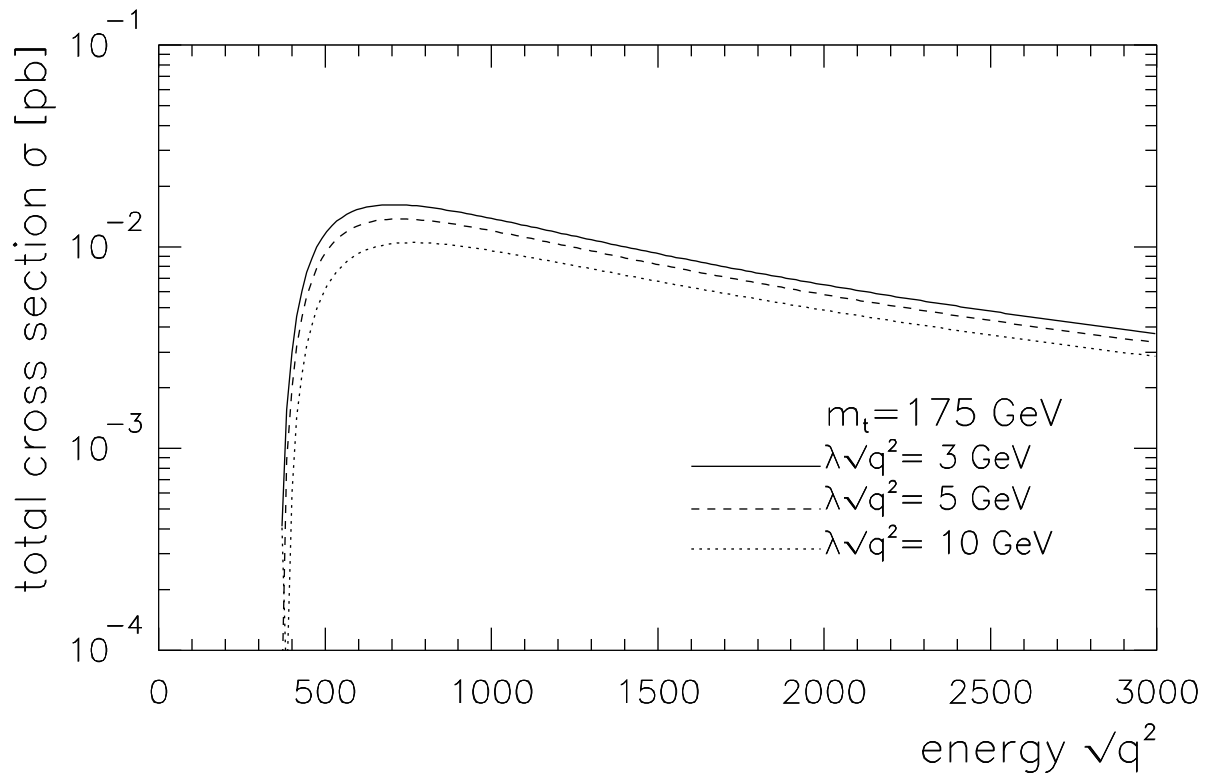


Figure 7(b)

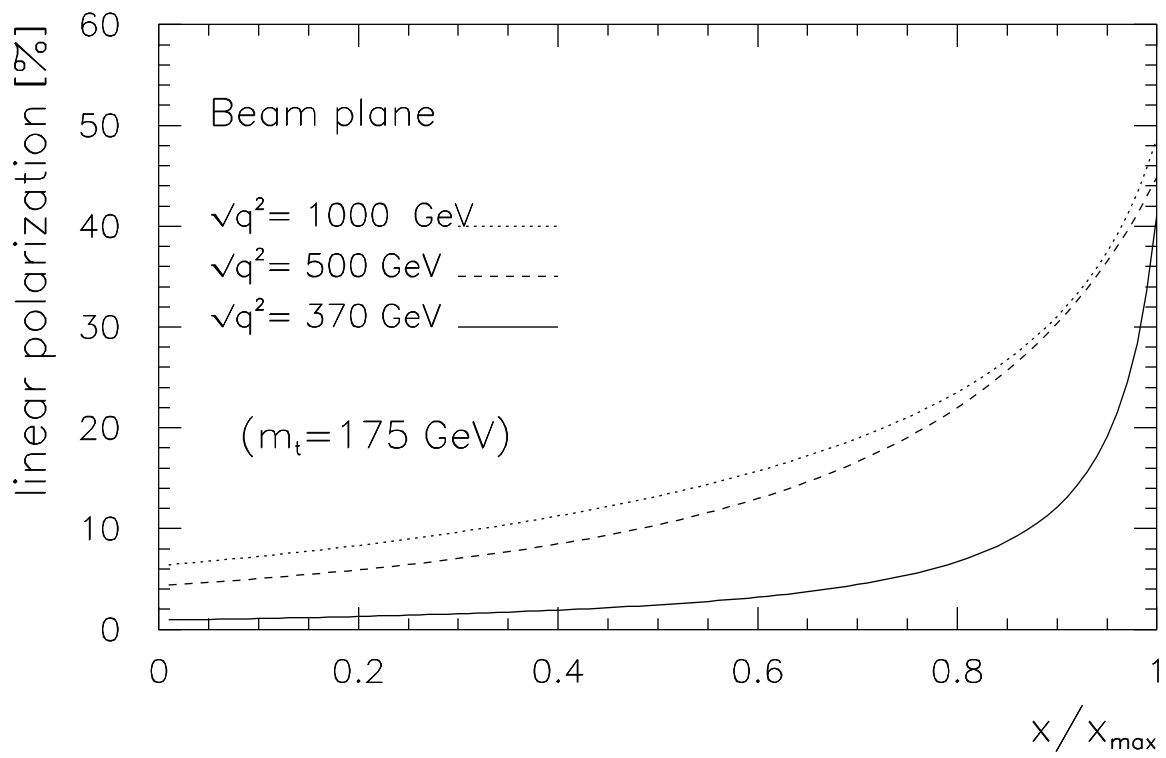


Figure 8

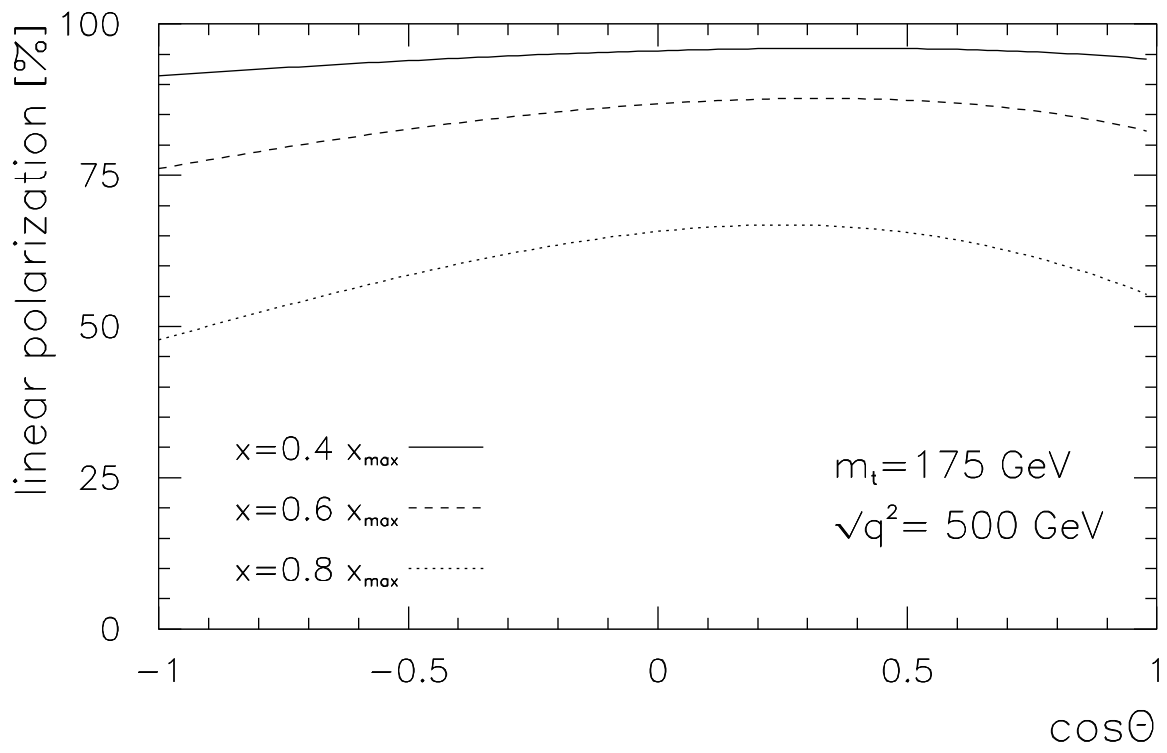


Figure 6(a)

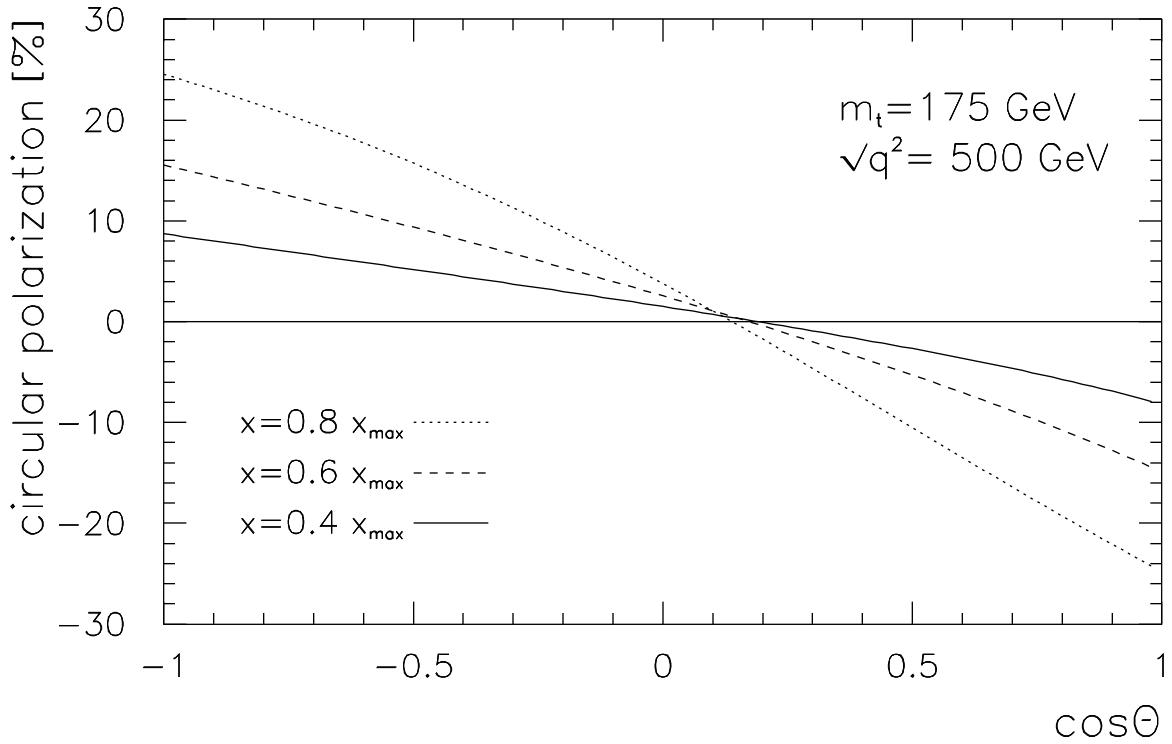


Figure 6(b)

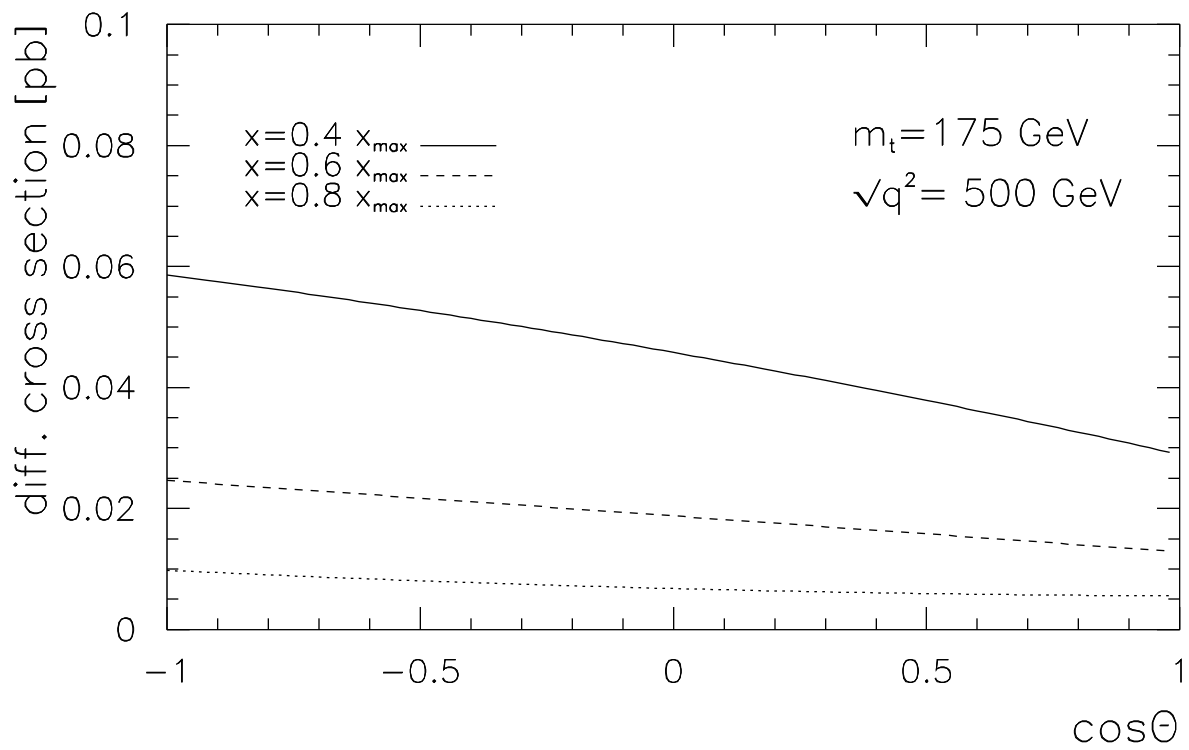


Figure 6(c)